

Theory of the Optical Properties of Lake Ice

PETER C. MULLEN AND STEPHEN G. WARREN

Geophysics Program, University of Washington, Seattle

A radiative transfer model is developed to illustrate the processes which determine the spectral albedo and transmission of lake ice. The calculated spectral albedo is dominated by specular reflection from the ice surface in the near infrared, whereas multiple scattering by bubbles below the surface dominates the visible albedo. Adding a snow cover to lake ice will normally increase the visible albedo, but may reduce the albedo in some regions of the near infrared if the sun is low, by reducing the specular reflection. In a preliminary test of the model, spectral albedo was measured on the natural ice cover of a frozen lake. The measurements are explained using the radiative transfer model applied to the air bubble size distribution measured in the same ice. The uncertainty in measurement of bubble size distribution leads to uncertainty in the theoretical albedo which is much larger than the error due to approximations used in derivation of the model.

1. INTRODUCTION

The reflection of sunlight from frozen lakes is largely controlled by the number and sizes of air bubbles, especially in the uppermost layers of the ice. In this paper we examine the link between the ice microstructure and the radiative properties, which have in the past usually been studied in isolation. The microstructure of lake ice, including porosity, crystal sizes and orientations, and bubble shapes, has been the subject of many studies. The only measurement of the spectral optical properties of lake ice was that of *Bolsenga* [1983]; however, the same principles apply to the optical properties of sea ice, which has received more attention [*Grenfell and Maykut*, 1977; *Grenfell and Perovich*, 1984] because of its role in global climate. We develop a model to explain the optical properties of lake ice in terms of its microstructure. What the model needs as input is the size distribution of air bubbles. We therefore also develop a method here for measuring that distribution.

2. STRUCTURE OF LAKE ICE

Following the initial freezing of a lake surface, ice is added to the bottom of the layer as heat is conducted upward through the ice. Air dissolved in the water cannot be incorporated into the ice crystal lattice; it remains in solution in the underlying water or, if the water is saturated with air, it appears as bubbles within the ice. The concentration of bubbles is larger when the freezing proceeds rapidly [*Gow and Langston*, 1977, Figures 16 and 17] because the boundary layer of water is then more readily saturated with air. However, the bubble concentrations in "congelation ice" thus formed by freezing at the bottom are generally quite small, so this ice is relatively clear and is often called "black ice" in contrast to the "white ice" or "snow-ice" which often subsequently forms above it.

Snow falling onto lake ice often becomes incorporated into the ice sheet by the invasion of liquid water into the air spaces between snow grains (forming slush) and subsequent freezing (forming snow-ice). As described by *Ragle* [1963] and *Adams* [1981], when cracks develop in the ice by thermal stress the water level rises in the cracks to its hydrostatic level which may be above the ice surface if there is sufficient snow cover.

The lake water floods the snow and incorporates nearly the entire snow layer as slush, as explained by *Knight* [1987, equations (1), (2), and (3)]. Water for the slush may also come from rain or from snow melt. Snow-ice can also be formed in the initial freezing event by snow falling into water at the freezing point. Snow-ice has small crystals and numerous spherical bubbles in dramatic contrast to the clearer, less bubbly, congelation ice below it. Snow-ice occupied less than half the total thickness of the ice, in the lakes studied by *Gow and Govoni* [1983] in New Hampshire and *Adams and Roulet* [1984] in Labrador.

Lake ice thus often consists of a very bubble "white" layer of snow-ice underlain by a clear layer of black ice. Many photographs of the surfaces of various ice types are given by *Wilson et al.* [1954]. The top surface of the ice, even if it consists of snow-ice, is usually flat enough to cause a specular reflection, so we must account for this in the theoretical model below.

In our modeling we treat the bubbles as spheres. The justification for this is as follows. Bubbles in snow-ice are generally spherical, and since snow-ice is the top layer it normally controls the albedo when it is present. In an environment of minimal snowfall the lake surface may contain only congelation ice, in which the bubbles form as vertical cylinders, sometimes called "worm bubbles" [*Swinzow*, 1966]. However, these cylinders metamorphose in time to strings of spheres [*Gow and Langston*, 1977, Figure 15] especially when the ice approaches 0°C throughout. In very cold climates, where the cylinders may retain their shapes, hoarfrost deposits on bubble walls [*Swinzow*, 1966, p. 34] and completely dominates the scattering of light, so even in this case it would not be useful to introduce the complexity of calculating the scattering by cylinders. We therefore as a first step, treat only spherical bubbles here. This is also appropriate for comparison with the field experiment described below, which was performed on snow-ice.

3. BUBBLE SIZE DISTRIBUTIONS IN NATURAL ICE

Size distributions of air bubbles in natural ice have rarely been measured. *Grenfell* [1983] measured the bubble size distribution in a sample of sea ice, which followed a power law: the number density $n(r)$ was proportional to $r^{-1.24}$, for radii r between 0.1 and 2.0 mm, and no bubbles were observed outside this range. *Grenfell's* Figure 3 shows that his distribution was similar to that measured by *Gavrilo and Gaitshkhoki*

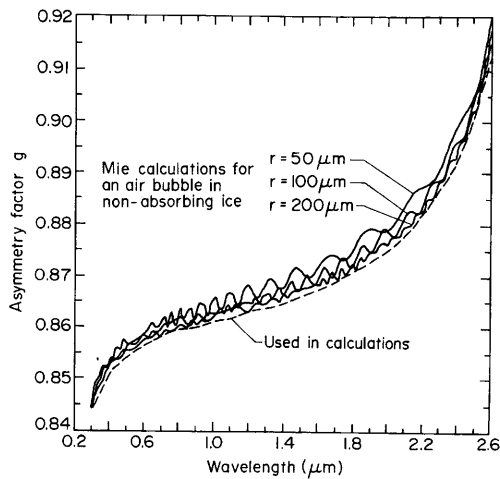


Fig. 1. Solid curves: single-scattering asymmetry factor as a function of wavelength for air bubbles of three different radii r , computed using Mie theory. The refractive index of the medium was assumed to be just the real part of the refractive index of ice; the imaginary part was set to zero. Dashed curve: approximate asymmetry factor $g(\lambda)$ used in multiple-scattering calculations.

[1970], who did not specify whether they were studying lake ice or sea ice. Gow and Langston [1977] examined bubbles in ice from a pond and a lake in New Hampshire several times during a winter. In one photomicrograph with a length scale, bubbles can be seen whose radii range from 0.1 to 1.0 mm. Their pictures illustrate the great variability of the sizes of bubbles in natural lake ice.

Although the processes by which air bubbles form in ice seem to be fairly well understood, the bubble size distributions that actually occur in natural lake ice have not been studied. We therefore use several different distributions in the model calculations.

4. SINGLE SCATTERING

4.1. Scattering in an Absorbing Medium

The single-scattering coefficients for a spherical particle depend on the wavelength of light, the radius of the particle, and the complex refractive index of the particle relative to that of the medium. Normally these coefficients are calculated using Mie theory. However, Mie theory may not be applicable to the case of an air bubble in ice, since in an absorbing medium the amount of light scattered by a single scatterer depends on the distance from it. The effect of absorption in the medium on scattering by the embedded particles has been studied by Chylek [1977] and Bohren and Gilra [1979], but only for the extinction efficiency. We need to develop approximations for both the scattering and absorption efficiencies, and also the phase function. How much the Mie results are modified by the introduction of absorption in the medium depends on the amount of absorption. In the visible spectrum, ice is fairly transparent so the Mie results (assuming no absorption) for the scattering efficiency Q_{sca} , and the scattering phase function are probably quite accurate. (Marston et al. [1982] have obtained good agreement with experiments of single scattering by air bubbles in liquid water at visible wavelengths (where the refractive index is similar to that of ice), completely ignoring the absorption by the medium.) At longer wavelengths (beyond about 1.4 μm), ice is more absorptive and Mie results probably are not correct. At these wavelengths, however, most of the light is absorbed before it has a

chance to be scattered so that the theoretical ice albedo turns out not to be much affected by an incorrectly calculated scattering coefficient. C. F. Bohren (personal communication, 1987) suggests the following criterion: Mie theory may be validly used for absorbing media when $k_{abs}^{-1} \gg L_{sca}$, where L_{sca} is the scattering mean free path.

4.2. Optical Constants of Pure Ice

The complex index of refraction m of ice as a function of wavelength λ has been compiled by Warren [1984]; m is a complex function, $m(\lambda) = m_{re}(\lambda) - im_{im}(\lambda)$, where m_{re} is the usual refractive index which determines the phase speed and m_{im} is related to the absorption coefficient of ice k_{abs}^{ice} as $k_{abs}^{ice} = 4\pi m_{im}/\lambda$, where λ is the wavelength in vacuum. The reciprocal of the absorption coefficient is the average distance a photon travels in pure bubble-free ice before being absorbed. At $\lambda < 0.8 \mu\text{m}$, radiation can travel several meters before being appreciably absorbed, while at $\lambda > 1.4 \mu\text{m}$ radiation is absorbed in less than a millimeter. The spectral variation of lake ice albedo is due to the variation of k_{abs}^{ice} with λ .

4.3. Scattering Coefficient

The scattering efficiency Q_{sca} is the ratio of the scattering cross section area of a particle to its geometric cross section area. For particles much larger than the wavelength, $Q_{sca} = 2.0$ [van de Hulst, 1957, p. 107]. This value is used in all the scattering calculations for bubbly ice, since the bubbles in the measured ice sample had radii $r \gg \lambda$. To argue for the plausibility of this simplification, Mie calculations were done for air bubbles in ice whose absorption was set to zero ($m = m_{re}$). These Q_{sca} varied between 2.00 and 2.05. This variation affects the spectral albedo of an ice layer by at most 0.005.

The scattering coefficient k_{sca} is the reciprocal of the average distance a photon travels through the bubbly ice before it is scattered. For a size distribution of scatterers $n(r)$,

$$k_{sca} = \int_0^{\infty} Q_{sca}(r) \pi r^2 n(r) dr \quad (1)$$

In our application, r is the radius of a bubble and $n(r)$ is the number of bubbles per unit volume per unit radius interval, with units $(\text{length})^{-4}$.

4.4. Asymmetry Factor

In the radiative transfer approximation we use below, it is not necessary to know the complete scattering phase function; only the asymmetry factor g is required, where g is the mean value of the cosine of the scattering angle (e.g., $g = 1$ for forward scattering and $g = 0$ for isotropic scattering). For large bubbles, g approaches a limiting value which depends on wavelength because m_{re} depends on wavelength.

To estimate an approximate value of $g(\lambda)$, Mie calculations are done in Figure 1 for bubbles in "nonabsorbing" ice; i.e., only the real part of $m(\lambda)$ is used, on the assumption that g is insensitive to negative m_{im} if $|m_{im}| \ll m_{re}$. In fact, the magnitude of m_{im} necessary to affect g significantly is much larger for negative m_{im} (absorbing medium, nonabsorbing particles) than for positive m_{im} (absorbing particles). For absorbing particles, values of m_{im} in the range 10^{-4} to 10^{-3} (ice at 1.5–2.5 μm wavelength) can cause g to increase significantly [Wiscombe and Warren, 1980, Figure 4]. However, this is due to attenuation of the rays which enter the particle, so that diffraction contributes relatively more than refraction to the phase function. An air bubble, by contrast, is essentially nonabsorbing at

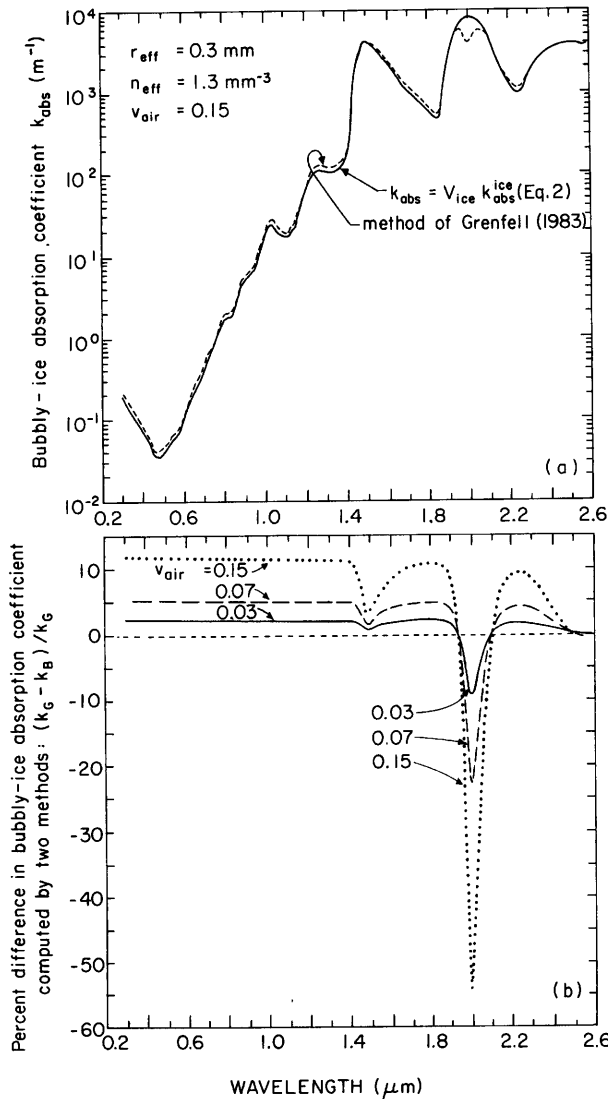


Fig. 2. (a) Absorption coefficient as a function of wavelength for bubbly ice computed by two methods as described in the text for a large volume fraction of air, $V_{air} = 0.15$. (b) Dotted curve: percent difference between the two curves in Figure 2a expressed as $(k_G - k_B)/k_G$, where k_G is k_{abs} from the method of Grenfell [1983] and k_B is k_{abs} from (2) (Bohren's method). Solid and dashed curves: percent difference in k_{abs} for smaller volume fractions of air.

4.5. Absorption Coefficient

Two techniques were tried for calculating the bubbly ice absorption coefficient k_{abs} . The first, which is used in our calculations below, was suggested by Bohren [1983]; it assumes that the absorption coefficient of the ice-air mixture is just that of pure ice (k_{abs}^{ice}) multiplied by the volume fraction of ice in the sample (V_{ice})

$$k_{abs} = V_{ice} k_{abs}^{ice} \tag{2}$$

The second, from Grenfell [1983], is to treat the absorption coefficient of bubbly ice as equal to the absorption coefficient of pure ice plus a (negative) absorption coefficient due to the air bubbles replacing some of the ice. Grenfell used Wiscombe's [1979, 1980] Mie code to calculate this negative absorption coefficient. Mie theory is not known to be valid for the case of negative imaginary index, but the numerical algorithms in the computer code remain stable (W. J. Wiscombe, personal communication, 1987). A negative absorption efficiency produces a negative absorption coefficient for bubbles, which causes the absorption coefficient for bubbly ice to be less than that of bubble-free ice, as it should be. Figure 2a displays the results of calculating k_{abs} with these two different techniques for ice containing 15% air by volume, in bubbles of radius 0.3 mm. A large volume fraction of air was used here to examine the differences between the two methods. This V_{air} is 5 times as large as V_{air} in the sample of snow-ice studied in our experiment below, but is not much larger than V_{air} found by Grenfell [1983] in sea ice.

The percentage difference between the two curves of Figure 2a is shown in Figure 2b, as well as the percentage difference for ice with smaller amounts of air. The greatest difference is at $\lambda = 2.0 \mu\text{m}$, where the absorption has a local maximum. At this wavelength the method of Grenfell can lead to negative k_{abs} for V_{air} greater than about 20%, which is obviously wrong, so we prefer the simpler approximation of Bohren. For the snow-ice studied in our experiment, with 3% air, the difference in albedo obtained by using the two alternatives for k_{abs} is at most 0.006.

4.6. Extinction Coefficient and Single-Scattering Albedo

The extinction coefficient k_{ext} , where

$$k_{ext} = k_{sca} + k_{abs} \tag{3}$$

is plotted in Figure 3 for several different bubble concentrations. At the short wavelengths, $k_{sca} \gg k_{abs}$, so that vari-

all wavelengths, so the only way that an imaginary part of the medium's refractive index could affect g is by changing the reflection coefficients and the angles of refraction, and this effect should not become significant at the 1% level until $|m_{im}| \geq 0.01 m_{re}$.

Figure 1 shows that for bubbles typical of lake ice (either snow-ice or congelation ice) g does not vary much with bubble size. In the model calculations below we therefore use a single smooth curve for g (dashed curve in Figure 1), allowing g to vary with wavelength but not with bubble size. This curve is drawn to approximate the large particle limit of g , since the effective radius for the size distributions we measure in lake ice (section 8 below) is about $300 \mu\text{m}$. This approximation leads to less than 0.01 error in g at all wavelengths, and about the same error in albedo (judging from Figure 19 of Wiscombe and Warren [1980], for $g < 0.92$), and saves considerable computation time.

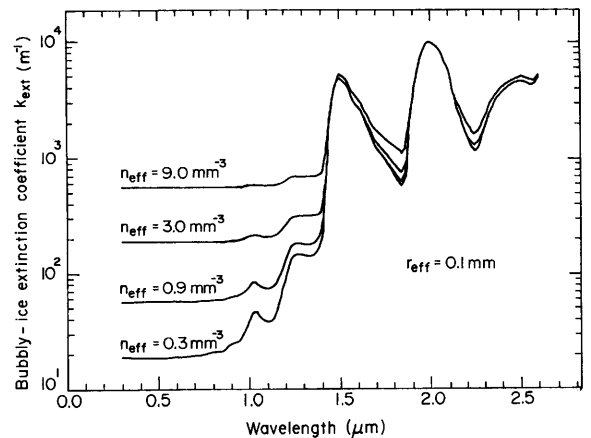


Fig. 3. Extinction coefficient as a function of wavelength for bubbly ice for four different number densities of bubbles, all with effective radius 0.1 mm.

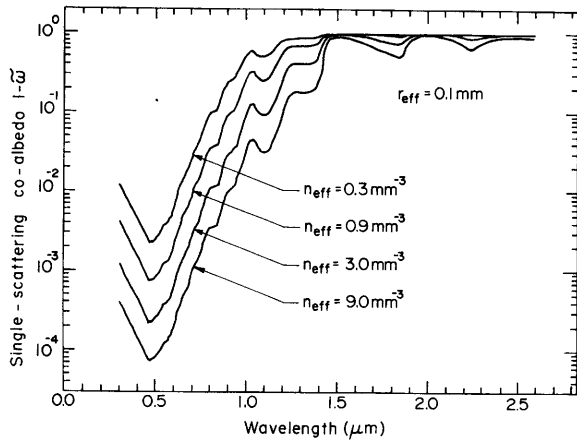


Fig. 4. Single-scattering coalbedo ($1 - \bar{\omega}$) as a function of wavelength for bubbly ice for four different number densities of bubbles, the same as used in Figure 3.

ations in bubble concentrations cause changes in extinction. At the longer wavelengths, absorption is dominant so that variations in the absorption coefficient with wavelength show up in k_{ext} .

The single-scattering albedo $\bar{\omega}$ is the probability that a photon will survive an extinction event:

$$\bar{\omega} = k_{sca}/k_{ext} \quad (4)$$

The single-scattering coalbedo ($1 - \bar{\omega}$) is plotted in Figure 4.

The optical depth τ is a dimensionless measure of the thickness of the layer

$$\tau = zk_{ext}$$

where z is the physical thickness of the layer; τ varies with wavelength because k_{ext} varies with wavelength.

5. MULTIPLE SCATTERING

An approximate solution to the radiative transfer equation is used to account for both multiple scattering in the bubbly ice and specular reflection due to the flat upper surface. Incorporation of the flat upper surface into the model was necessary for the snow-ice of the experiment described below; it might not be appropriate for very rough lake ice surfaces. For scattering within the ice we use the delta-Eddington method [Joseph et al., 1976; Wiscombe and Warren, 1980]. The delta Eddington method was designed to make accurate yet rapid calculations of radiation fluxes in media whose scattering phase functions are highly peaked in the forward direction. This situation applies when the particle size is much larger than the wavelength, in particular for clouds and snow, as well as for air bubbles in lake ice, at solar wavelengths. It is a modification of Eddington's approximation (essentially a two-stream approximation) in conjunction with a truncation of the forward peak of the single-scattering phase function. Photons, which are only slightly deflected from the forward direction are considered to be unscattered. The remaining altered phase function is then much less asymmetric, and within the domain of validity of Eddington's approximation. The incorporation of internal and external specular reflection at the upper ice surface leads to what we call the "specular delta-Eddington" method, as follows. (Reflection at the ice-water interface is assumed negligible because ice and water have nearly identical refractive indices at solar wavelengths.) This general approach has been used before by Saunderson [1942], who used a two-stream approximation for the medium below the interface,

and in ocean optics, for example, by Tanaka and Nakajima [1977], who used the doubling method for the scattering medium.

The albedo a is the ratio of upward irradiance F^{up} to downward irradiance F^{down} just above the surface. We first consider the case where F^{down} is just a direct beam from the sun at zenith angle θ_0 with cosine μ_0 .

The upward irradiance is the sum of a number of components

$$F^{up} = \sum_i F_i^{up}$$

listed as follows.

1. External specular reflection ($i = 1$):

$$F_1^{up} = R_1 F^{down}$$

where R_1 is the external specular reflection coefficient (air to ice).

2. Transmission into ice, scattering by bubbles and transmission up out of the ice ($i = 2$):

$$F_2^{up} = F^{down}(1 - R_1)A(\theta_1)(1 - R_2)$$

where R_2 is the internal reflection coefficient (ice to air) and $A(\theta_1)$ is the multiple-scattering delta-Eddington albedo for a direct beam at the angle θ_1 given by Snell's law: $\sin \theta_0/\sin \theta_1 = m_{re}(\lambda)$.

3. Transmission into ice, scattering by bubbles, internal reflection from the top surface back into the ice, scattering again by bubbles and transmission up out of the ice ($i = 3$):

$$F_3^{up} = F^{down}(1 - R_1)A(\theta_1)R_2A_d(1 - R_2)$$

where A_d is the multiple-scattering delta-Eddington albedo for the field of internally reflected radiation. The internally reflected radiance has a strong angular dependence. This diffuse reflection A_d is calculated by numerically integrating over angle the delta-Eddington albedo weighted by the internally reflected radiation field.

4. The remaining terms ($i = 4, 5 \dots$) contributing to F^{up} are identical to F_3^{up} but multiplied by higher powers of R_2A_d , corresponding to multiple reflections of radiation between the scattering layer and the top surface. The albedo $a = F^{up}/F^{down}$ is thus an infinite series

$$a = R_1 + (1 - R_1)A(\theta_1)(1 - R_2)[1 + R_2A_d + (R_2A_d)^2 + \dots]$$

which can be summed as

$$a = R_1 + \frac{(1 - R_1)A(\theta_1)(1 - R_2)}{(1 - R_2A_d)} \quad (5)$$

This is the albedo for a direct beam at θ_0 . In general, F^{down} contains contributions from other parts of the sky in addition to the solar beam; in that case the albedo from (5) is numerically integrated over θ_0 .

6. BEHAVIOR OF THE MODEL

The addition of a flat surface on the top of a scattering layer affects the total albedo a in three ways. First, the external surface reflectance tends to increase the total albedo over what it would be without the surface layer, but second, the internal reflection directs radiation back down into the scattering layer where it has another chance to be absorbed, tending to decrease the total albedo. The latter effect has little dependence on the zenith angle of the incident radiation, but the former

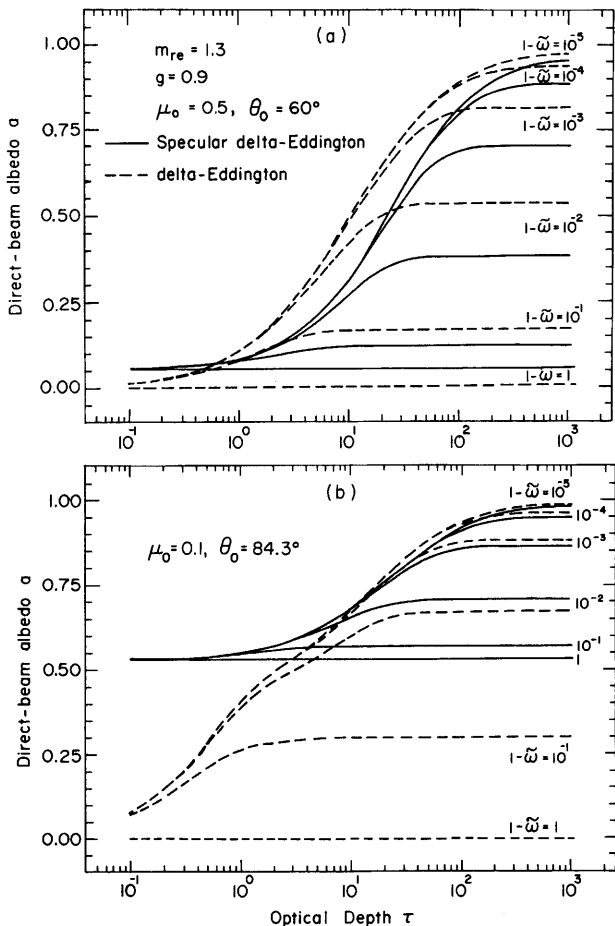


Fig. 5. Albedo as a function of total optical depth of the layer for six different values of single-scattering albedo. Dashed curves: delta-Eddington method used for multiple-scattering calculations. Solid curves: specular delta-Eddington method used (i.e., reflection at upper surface included). (a) Solar zenith angle = 60° . (b) Solar zenith angle = 84.3° .

effect has a strong zenith angle dependence, so that at small zenith angles the albedo is reduced and at large zenith angles it is increased, relative to the case with no surface layer. The angle at which the two effects are equal depends on the properties of the scattering layer and is discussed by Mullen [1984]. A third effect that tends to reduce the total albedo is the refraction of the direct beam to a smaller incident angle as it enters the scattering layer, because the albedo of the scattering layer increases with angle of incidence. Figure 5 compares the results of "specular" to standard delta-Eddington calculations. The somewhat surprising result is that addition of the interface reduces the total albedo over a significant range of ice thickness, generally for $\tau > 1$ at $\theta_0 = 60^\circ$ and at $\tau > 10$ at $\theta_0 = 84.3^\circ$.

This is shown in another way in Figure 6, which shows the albedo for isotropic incident radiance (the "diffuse albedo") for a semi-infinite scattering layer. The diffuse albedo is calculated by integrating the direct beam albedo over angle. In this case, if the delta-Eddington albedo is greater than about 0.1, addition of specular reflection reduces the total albedo.

The idea of using the delta-Eddington method for a scattering layer below a reflecting interface was criticized by Houf and Incropera [1980], so we should explain why it has worked successfully for us. In the cases which are of interest in lake ice (no bottom reflection, optically thick, large single-scattering

albedo) Houf and Incropera's plots show that delta-Eddington gave suspension plus bottom reflectances (i.e., not including external reflection) closer to the more exact discrete ordinates method than did the other rapid approximate methods they tested. Their pessimism about the utility of the delta-Eddington method thus does not find support in their figures for the case of lake ice. Furthermore, the version of the delta-Eddington method they chose to criticize has important deficiencies compared to the method we are using, because they included the internal reflection at their air-water interface as a boundary condition when deriving the delta-Eddington formulas. As they noted, this technique "precludes accounting for the concentration of the diffuse irradiation due to refraction at the air-water interface." It also cannot account for the redistribution of the radiance field when it is internally reflected by the interface. Both effects are included in the formulation we use.

Our theory uses several approximations where more detailed computations could be done. These approximations include the use of a constant value for Q_{sca} independent of wavelength and bubble size, an asymmetry factor independent of bubble size, the formula for the absorption coefficient of bubbly ice, and the delta-Eddington approximation. The justification for each approximation is that the approximation introduces less error into the calculations than does the uncertainty in the measurement of air bubble size distribution, which as we will see below is the major cause of uncertainty in the albedo of natural ice.

7. SPECTRAL ALBEDO CALCULATIONS

7.1. Bubble Size Distribution Parameterization

Here we show that for radiative purposes, any size distribution of bubbles can be described by just two parameters. Only one parameter, an effective radius, is normally needed for clouds [Hansen and Travis, 1974] or snow, where the same particles are responsible for both scattering and absorption. In lake ice, where scattering is by air but absorption is by ice, two parameters are needed. An effective bubble concentration n_{eff} and an effective bubble radius r_{eff} can be found that will produce the same single-scattering quantities as any given distribution of spherical bubbles, provided that the bubbles are all large compared to the wavelength. Since g is nearly independent of particle size (Figure 1) and k_{abs} is nearly indepen-

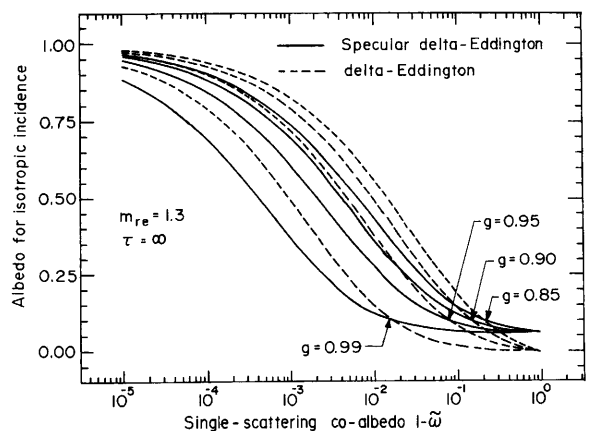


Fig. 6. Albedo of semi-infinite layer for isotropic incidence as a function of single-scattering coalbedo for four different values of asymmetry factor g , including (solid curve) or excluding (dashed curve) specular reflection at the upper surface.

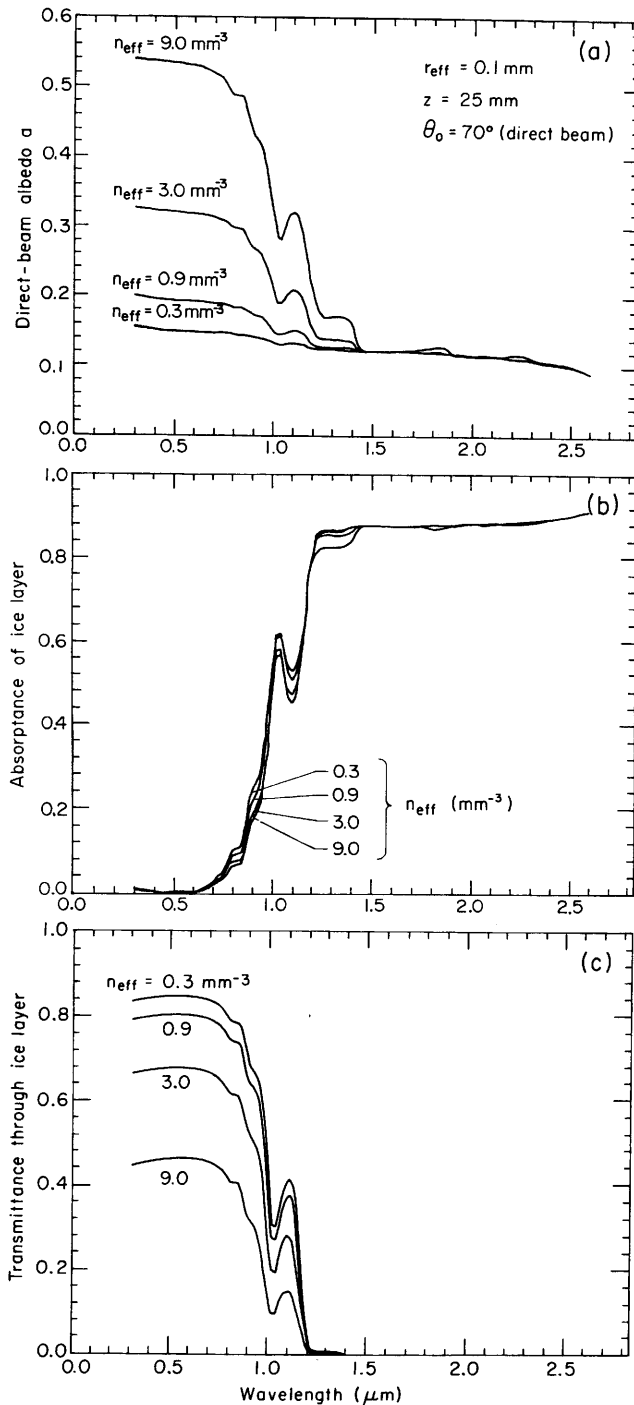


Fig. 7. Albedo, absorbance, and transmittance as functions of wavelength for an ice layer of thickness 25 mm for four different number densities of bubbles.

dent of particle size and number density, or air volume (for air fractions typical of lake ice; see discussion of Figure 2), it is sufficient to find n_{eff} and r_{eff} such that k_{sca} is the same as for the actual distribution. The volume fraction of air is

$$V_{air} = \int_0^{\infty} \frac{4}{3} \pi r^3 n(r) dr = \frac{4}{3} \pi r_{eff}^3 n_{eff} \quad (6)$$

and the scattering coefficient for the size distribution, from (1), setting $Q_{sca} = 2$, is

$$k_{sca} = \int_0^{\infty} 2\pi r^2 n(r) dr = 2\pi r_{eff}^2 n_{eff} \quad (7)$$

Solving for n_{eff} and r_{eff} gives

$$r_{eff} = 3V_{air}/2k_{sca}$$

$$n_{eff} = (2k_{sca}^3/\pi)/(3V_{air})^2$$

Since any size distribution of bubbles much larger than the wavelength of light can thus be simply characterized by its effective radius and concentration, we need show only calculations for ice with bubbles of uniform size. Since various combinations of n_{eff} and r_{eff} can give the same ice density, density is not useful as a predictor of optical properties.

7.2. Sensitivity to Bubble Size and Concentration, Ice Thickness, and Zenith Angle

We change these variables one at a time from a "standard" case, which corresponds approximately to the ice layer studied in the field experiment below, with $r_{eff} = 0.3$ mm, $n_{eff} = 0.3$ mm⁻³, $\theta_0 = 70^\circ$, and ice thickness $z = 25$ mm. Some figures use $r_{eff} = 0.1$ mm, which applies to the bubble size distributions measured in the laboratory by *Carte* [1961] and *Bari and Hallett* [1974] for freezing rates similar to those found in lakes.

Figure 7a shows the albedo for various bubble concentrations, keeping ice thickness and r_{eff} fixed. The number density n_{eff} is varied from the standard value (0.3 mm⁻³) upward to 9 mm⁻³, which results in albedo approaching that of snow so would correspond to very bubbly snow-ice. We do not vary n_{eff} in Figure 7 to values lower than 0.3 mm⁻³ because at that concentration the albedo approaches that of bubble-free ice. The corresponding scattering coefficients (as well as those for other figures) are shown in Table 1; they are independent of wavelength. At the longer wavelengths, the reflection is essentially due to specular reflection from the surface because any light that enters the ice is almost certain to be absorbed. At shorter wavelengths the scattering of light by bubbles raises the albedo over that due to specular reflection alone. The peaks and valleys in the spectral albedo curve correspond to minima and maxima, respectively, in the absorption coefficient of pure ice. More bubbles or larger bubbles cause the albedo to increase at all wavelengths because (1) k_{sca} increases, so $\tilde{\omega}$ increases, (2) optical thickness is greater, and (3) k_{sca} is slightly smaller (but since the volume fraction of ice is always close to unity, this last effect is normally insignificant compared with the other two). Figures 7b and 7c show the absorbance and transmittance of the ice; these figures will be discussed below.

Figure 8 shows the effect of ice thickness. At $\lambda > 1.2$ μm the albedo is just due to specular reflection and is independent of thickness. The peak in albedo at 0.5 μm is less sharp for thin ice than for thick ice. In an infinitely thick layer of bubbly ice, some photons follow a long path through the ice before they reemerge at the top surface. With such a long path through the ice, some photons are absorbed at all wavelengths, but fewer where k_{abs} is smallest, so the albedo has a peak at this wavelength. In a thin ice layer (less than about 100 mm for the bubble population of Figure 8) a photon is scattered only a few times by bubbles inside the ice, and then exits the layer, either through the top or the bottom. The total length of the path followed by a photon in the ice is shorter than in the infinite case, and there is a range of wavelengths for which absorption by ice is small enough that photons will essentially not be absorbed in the ice (as shown in Figure 7b and discussed in section 7.5 below), so the albedo is nearly constant in this range of wavelengths. (This behavior is also seen for thin snow in Figure 13 of *Wiscombe and Warren* [1980].) The albedo peak would also be broadened in thick ice if n_{eff} were

TABLE 1. Properties of Bubble Size Distributions Used in Calculations

| Figure No. | r_{eff} , mm | n_{eff} , mm ⁻³ | k_{sca} , m ⁻¹ | V_{air} | ρ , g cm ⁻³ |
|-------------------------------|----------------|------------------------------|-----------------------------|-----------|-----------------------------|
| 2 | 0.3 | 0.3 | 170 | 0.034 | 0.886 |
| 3, 4, and 7 | 0.1 | 9.0 | 565 | 0.038 | 0.882 |
| | 0.1 | 3.0 | 188 | 0.013 | 0.905 |
| | 0.1 | 0.9 | 57 | 0.0038 | 0.913 |
| | 0.1 | 0.3 | 19 | 0.0013 | 0.916 |
| | 0.3 | 0.3 | 170 | 0.034 | 0.886 |
| 8, 9, 11, and 12 | 0.07 | 21.0 | 647 | 0.03 | 0.89 |
| | 0.2 | 0.9 | 226 | 0.03 | 0.89 |
| | 0.7 | 0.02 | 62 | 0.03 | 0.89 |
| 15 and 16 | 0.3 | 0.54 | 305 | 0.06 | 0.861 |
| | 0.33 | 0.24 | 164 | 0.036 | 0.884 |
| Grenfell [1983] | 1.28 | 0.008 | 82 | 0.07 | 0.852 |
| Gavrilo and Gaitskhoki [1970] | 1.28 | 0.014 | 144 | 0.12 | 0.804 |

Here, r_{eff} is the effective radius of the bubble size distribution, n_{eff} is the effective number density of bubbles, k_{sca} is the scattering coefficient of the bubbly ice, V_{air} is the volume-fraction of air, and ρ is the density of the bubbly ice.

so large that essentially all photons were scattered up out of the ice with a very short total path length through the ice. The albedo then would be very close to 1.0 for a range of wavelengths.

Figure 9 shows the effect of solar zenith angle on albedo. Both the specular reflection and the delta-Eddington albedo increase with zenith angle. These calculations are for a mono-directional beam; the actual variation of albedo with sun angle under natural illumination would be weaker than shown here, because of diffuse light from Rayleigh scattering.

Figure 10 demonstrates that ice density (or porosity) is not useful as a predictor of albedo. It shows how the albedo changes if the bubble sizes change while fixing the total air content. Ice with many small bubbles has higher albedo than ice (of the same density) with a few large bubbles.

7.3. Sensitivity to Approximations Made in the Theory

Although all the albedo calculations used a scattering efficiency of 2.0, Mie calculations show that the scattering efficiency ranges between 2.00 and 2.05. The albedos calculated using these two extreme values differ by less than 0.01. The error in albedo due to the use of a parameterization for g

(Figure 1) is also 0.01 or less, and the difference in albedo due to the use of two alternative methods of computing k_{abs} is also less than 0.01 (if $V_{air} < 0.03$). Uncertainty in r_{eff} , which can cover the range of sizes used in Figure 10, thus leads to greater error in albedo than do the approximations for the single-scattering quantities.

The error in albedo due to an approximate method for multiple scattering is also small. The delta-Eddington method is known to underestimate the albedo of a homogeneous layer at large zenith angles [Joseph *et al.*, 1976, Figure 3]. But because specular reflection from the top of the flat ice surface becomes very large as $\theta \rightarrow 90^\circ$, little light enters the multiple-scattering medium, so the scattering by bubbles (where delta-Eddington is used) contributes only a small fraction of the total albedo.

We do not invoke the presence of absorptive impurities in the ice to explain its optical properties, as was necessary for snow [Warren and Wiscombe, 1980]. Parts-per-million amounts of impurities such as dust or soot can significantly reduce the albedo of snow only in spectral regions where the albedo of pure snow is greater than about 0.7. Such high albedos are not normally encountered at any wavelength for sea ice [Grenfell and Perovich, 1984, Figure 3] or lake ice

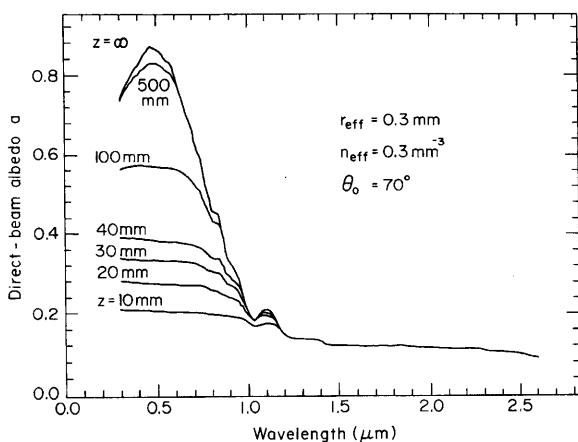


Fig. 8. Effect of ice layer thickness z on spectral albedo of bubbly ice.

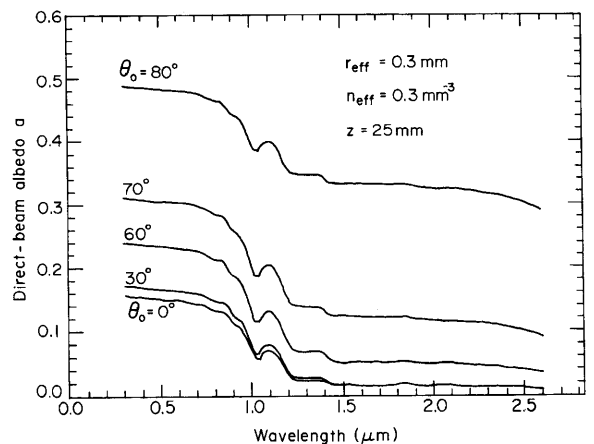


Fig. 9. Effect of solar zenith angle θ_0 on spectral albedo of bubbly ice.

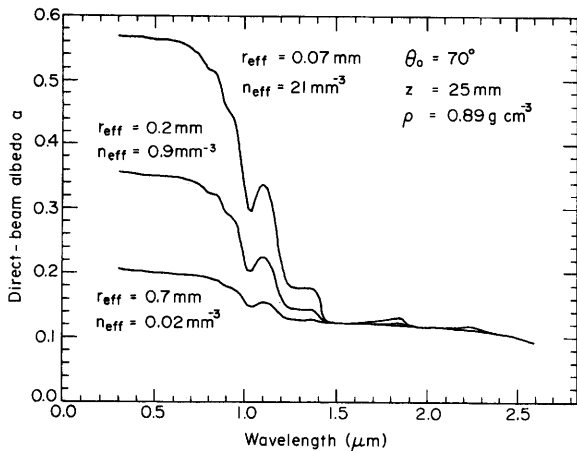


Fig. 10. Spectral albedo of an ice layer with density 0.89 g cm^{-3} , with three different bubble size distributions. All three ice layers have the same volume fraction of air, so the number density of bubbles n_{eff} is smaller for the case of larger effective radius r_{eff} .

(Bolsenga [1983]; and final figure of this paper) unless they are covered with snow, a case which is treated in the next section.

The model used in this paper may be compared with the simpler theory used by Bohren [1983] to explain the colors of frozen waterfalls. For Q_{sca} and k_{abs} he used the same approximations we use ($Q_{sca} = 2.0$; $k_{abs} = V_{ice}k_{abs}^{ice}$); the principal difference is in the multiple-scattering theory. The radiative transfer approximations of Bohren are valid only for visible wavelengths, where $k_{sca} \gg k_{abs}$, so to compare his results with ours we instead use Bohren [1983, equation 6] for $\bar{\omega}$ together with Bohren [1987, equation 28] for albedo, which is not restricted to visible wavelengths. In Figure 11 we compare our results with those of the simpler theory for the case of isotropic incidence on a semi-infinite layer (which Bohren's (28) assumes), using a reasonable bubble distribution ($r_{eff} = 0.3 \text{ mm}$; $n_{eff} = 0.3 \text{ mm}^{-3}$). Bohren's albedo is close to the delta-Eddington albedo without specular reflection. The simple method based on Bohren's equations is seen to be perfectly

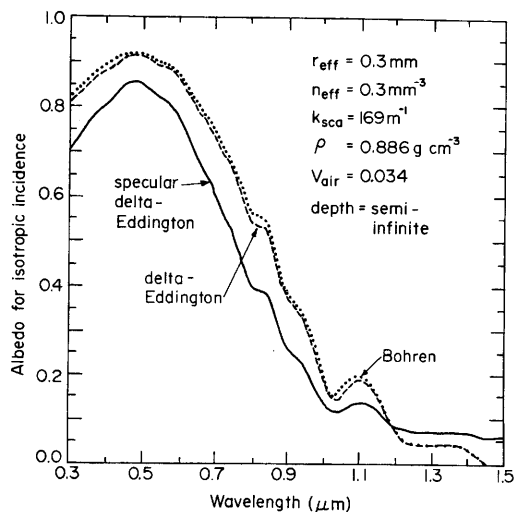


Fig. 11. Spectral albedo (for isotropic incidence) of semi-infinite layer of bubbly ice computed using Bohren's [1987] method, compared to results of delta-Eddington and specular delta-Eddington methods. The specular delta-Eddington is the most accurate if the ice has a flat upper surface.

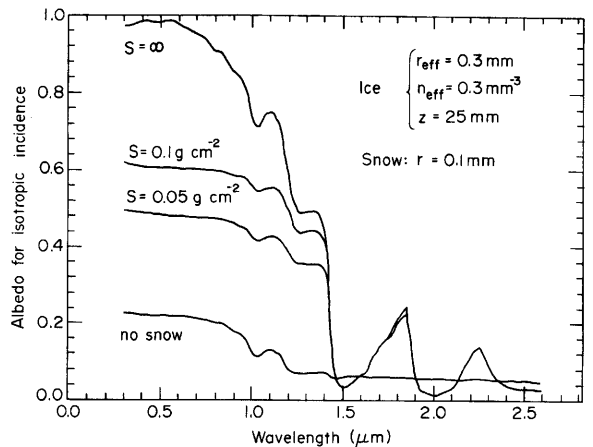


Fig. 12. Spectral albedo (for isotropic incidence) of bubbly ice covered with a snow layer of thickness s .

adequate for the case of no specular reflection (which might be appropriate if the ice surface is very rough).

7.4. Snow-Covered Ice

Lake ice and sea ice are often covered by snow. We model this as a multiple-layer system, and calculate the albedo for isotropic incidence (the "diffuse albedo"). (The diffuse albedo turns out empirically to be about the same as the albedo for a direct beam at $\theta_0 = 62^\circ$.) First the diffusivity albedo of the ice layer is calculated, to be used as a lower boundary condition for the calculation of the snow albedo. The snow albedo is then calculated by the method of Wiscombe and Warren [1980] for different thicknesses s of snow. Figure 12 shows that a small amount of snow dramatically increases the albedo of the snow/ice system at most wavelengths. Only near 1.5 and 2.0 μm does the snow actually cause the albedo of the system to decrease. At these wavelengths, the absorption in the snow is very strong and little light is scattered out, but there is still reflection from the flat surface of the ice. We know of no observations to date which have confirmed this. Albedos of sea ice measured by Grenfell and Perovich [1984] were no larger than those of snow at 1.5 and 2.0 μm ; however, errors in albedo are large at these wavelengths because there is little solar energy flux.

7.5. Absorption of Light in the Ice

Figures 7b and 7c show the absorptance and transmittance of ice with different bubble concentrations; the sum of the three values in the three parts of Figure 7 add to 1.0 at each wavelength. These calculations were done using the same principles described above. From the Eddington approximation, a formula for absorption can be obtained [Irvine, 1975]. The delta function modification is applied following Joseph et al. [1976]. Finally, the multiple reflection technique described above is used to obtain the absorptance of a layer of lake ice. Figure 7b shows that the total absorption in ice of 25 mm thickness is sensitive to the bubble concentration only between 0.8 and 1.4 μm wavelength. At longer wavelengths, all the light that enters the ice is absorbed, and in the visible none is absorbed; it is either transmitted or reflected. Of course, if the ice were very thick, then there would be no transmission at any wavelength and the absorption plus the albedo would add to 1.0. At longer wavelengths there is no transmission and almost no scattering by bubbles, so the absorptance plus the surface reflectance add essentially to 1.0.

8. EXPERIMENT

Two measurements were made of the spectral albedo of ice on Moses Lake in central Washington State (47°N, 119°W) in 1984 and 1985. The lake's dimensions are about 10 km east-west and 15 km north-south. The experiment was done on a narrow arm extending from the northern end of the lake. Samples of the ice were brought to a cold room for measurement of bubble sizes. Ice on this and nearby lakes is usually covered with snow; the snow-free ice studied here had actually been artificially cleared of snow. Only the 1984 experiment is discussed here because the ice from the 1985 experiment was lost due to a refrigeration failure before the bubble sizes were measured.

8.1. Radiation Measurements

The photometer used for the radiation measurements [Grenfell, 1981] is capable of measuring irradiance in narrow spectral intervals (resolution 20–100 nm) from 0.4 to 2.5 μm , using interference filters. It measures the radiation flux from a hemisphere, employing a "cosine collector" to properly weight the radiance from all angles. It can be easily flipped over to measure incident and reflected radiation fluxes alternately. A correction for shadowing of the ice by the instrument is about 1% for diffuse incidence and much less for direct beam incidence. The solar zenith angle was calculated by the method of Walraven [1978] with the corrections of Wilkinson [1981]; it varied between 69 and 75 degrees during the course of the experiment on January 17, 1984.

8.2. Measurement of Bubbles

A coring drill was used to obtain samples of the ice directly below the photometer after the radiation measurements had been made on Moses Lake. The top layer was 25 mm of snow-ice with numerous spherical bubbles, which was underlain by 200 mm of relatively bubble-free ice. The ice cores were 100 mm in diameter and 100–150 mm long. The bubbles seemed to be distributed uniformly throughout the top layer; there were no obvious internal layers or inhomogeneities.

The bubble size distribution was measured by taking photomicrographs (e.g., Figure 13) of vertical thin sections of the ice sample (~ 1 mm thick) and then measuring the diameter of the bubbles with the photomicrographs projected onto a digitizing table. This technique just gives a measure of the area density of bubbles in the ice because it is only a two-dimensional image. The area density was converted to a volume density by assuming that only the bubbles which appeared in focus were counted. Bubbles would appear to be in focus if they were located within a small definite distance of the plane of focus. The thickness of this "in-focus layer" was determined experimentally by moving the microscope up and down and measuring the difference in height of the microscope between when a bubble came into focus and when it went out of focus. The decision as to whether a bubble appears in or out of focus in a photomicrograph is subjective, so the focus calibration and the bubble measurements were both done by the same person. Figure 14 shows that larger bubbles appeared in focus over a larger distance than did smaller bubbles. The data points are bracketed by the upper and lower lines, referred to as thick- and thin-focus calibrations, which are used later to obtain two extreme estimates of the bubble size distribution which should bracket the true distribution.

The diameter of each bubble examined was calculated from the digitized data. The size distribution was determined by

dividing the bubbles into 18 bins according to size (18 bins is sufficient to describe the size distribution; subdivision into more bins would lead to larger statistical errors in $dN/d \log r$ because of smaller counts in each bin) and dividing the number of bubbles in a bin by the width of the bin and the volume in which the bubbles had been found. The two distributions obtained, corresponding to the thick- and thin-focus calibration, are shown in Figure 14. Each data point is from the count in a size bin. The width of the point indicates the width of the size bin and the height indicates the uncertainty in the count (the square root of the count). This figure shows that the uncertainty associated with the counting process is less than the uncertainty associated with the "focus thickness" calibration.

The bubbles ranged from 0.007 to 0.8 mm radius with the peak of the distribution at 0.06 mm. The limit of the resolving power of the counting technique is about 0.007 mm. However, the trend in the distribution curve in Figure 14 indicates that smaller bubbles would be few in number. A large number of bubbles too small to count would still scatter light and cause the ice to appear cloudy under the microscope. Since the interbubble ice appeared clear under the microscope, we know that the smallest bubbles that are important scatterers were counted. There were also a few larger bubbles up to several mm radius that could be seen in the ice without a microscope, but they never happened to be in the photomicrographs. The parameters which result from these size distributions are summarized in Table 1 under the entry for Figures 15 and 16.

8.3. Comparison of Theory and Experiment

During the 2-hour period during which the field measurements were taken, the solar zenith angle was changing. The sun angle at the time of measurement of a particular wavelength was used in the albedo calculation for that wavelength, plotted in Figure 16, so these curves differ from the theoretical curves displayed earlier. The two curves in Figure 16 were calculated using the bubble distributions from Figure 15. Unfortunately, the photometer's wavelength determination system began to fail at the end of the experiment so that the wavelength for the reflected measurement was not exactly the same as the wavelength for the incident measurement. This is the cause of the scatter in the experiment data at wavelengths less than 0.7 μm . (Although albedo should be rather constant from 0.4 to 0.7 μm , the solar irradiance and the sensitivity of the silicon photodiode are not constant with wavelength, so accurate wavelength positioning is essential.) At visible wavelengths, the theoretical curves surround the data points even with the scatter caused by the malfunctioning of the instrument. At $\lambda > 1.4 \mu\text{m}$ the measurements are very close to the calculated values: here the albedo is just due to surface reflection so is the same for both bubble size distributions.

At 0.8–1.1 μm the calculations overestimate albedo if we assume the true bubble size distribution is intermediate between the "thick-focus" and "thin-focus" distributions. At these wavelengths, light travels through ice on average a distance on the order of the thickness of the bubbly ice layer before being absorbed. Therefore the albedo is most sensitive to the bubble size distribution close to the top surface. The discrepancy could therefore be resolved if above the bubbly layer there were a layer of clear ice several mm thick, because the albedo would be reduced in this spectral region but unaffected in the visible region. However, visual inspection of the



Fig. 13. Photograph of a vertical thin section of the top layer of ice from Moses Lake, January 17, 1984.

ice core did not show a clear layer or even a smaller bubble density at the very top.

The discrepancy may be due to experimental error related to the low sun, because the calibration for the cosine collector varies rapidly with zenith angle when the sun is close to the horizon. The cosine collector used here has been well calibrated only for $\lambda < 0.8 \mu\text{m}$. (This problem was avoided in the 1985 experiment by making measurements under diffuse lighting conditions where it is much less important to know the cosine calibration, but as mentioned, the ice samples from that experiment melted prematurely.) Furthermore, there is sub-

stantial diffuse radiation from the sky when the sun is low, and its distribution was unknown; this is an additional source of error in the modeling. We conclude that this experiment did not identify flaws in the model.

9. CONCLUSION

Model calculations show that the spectral albedo of lake ice depends on the bubble size distribution, the absorption coefficient of ice, the solar zenith angle, and the thickness of the bubbly layer. Ice density is not a useful predictor of the albedo. The visible albedo is dominated by scattering of light

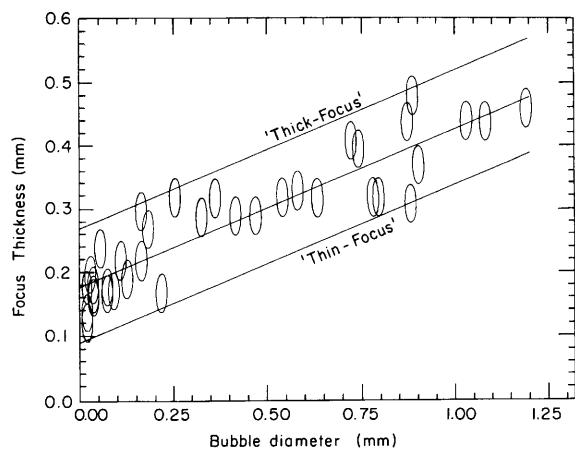


Fig. 14. Calibration curve for estimation of bubble size distribution by microscope. The vertical axis (focus thickness) is the maximum distance through which the microscope lens could be moved while the bubble appeared to remain in focus. The plotted points are the observations; the thick- and thin-focus lines are drawn so as to bracket the observations and are used below as the uncertainty in focus thickness. In the measurement of size distribution, all bubbles which appeared to be in focus were counted, then the sum was divided by the focus thickness (from this figure) and the viewing area to obtain the number density.

within the ice which is controlled by the number and size of bubbles and how they are distributed with depth. The albedo beyond $1 \mu\text{m}$ is dominated by reflection from the surface which is controlled by the solar zenith angle.

The calculations show great sensitivity of visible albedos to the size distribution of bubbles. Even the uncertainty in the measurement of a bubble size distribution in the experiment introduces an uncertainty of 0.1 in the calculated visible albedo. Little work has been done on actually determining bubble size distributions in natural lake ice and sea ice. Because of this sensitivity and uncertainty, it is probably not useful to assume a standard bubble distribution when attempting to calculate the climatological radiative properties of lake ice or sea ice. It is also probably inappropriate to do single-scattering calculations more accurately than with the approximations used here when the subtle effects that these

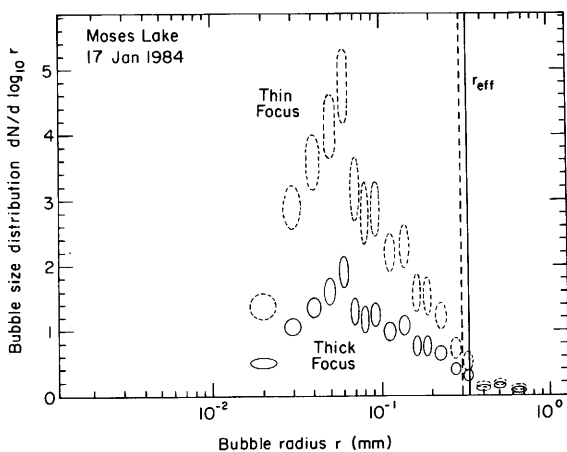


Fig. 15. Size distribution of bubbles in the ice on Moses Lake whose spectral albedo was measured on January 17, 1984. The two size distributions result from the two extreme assumptions of focus thickness shown in Figure 14; the true distribution should be intermediate between these two extremes. Vertical lines show the effective radii for these distributions.

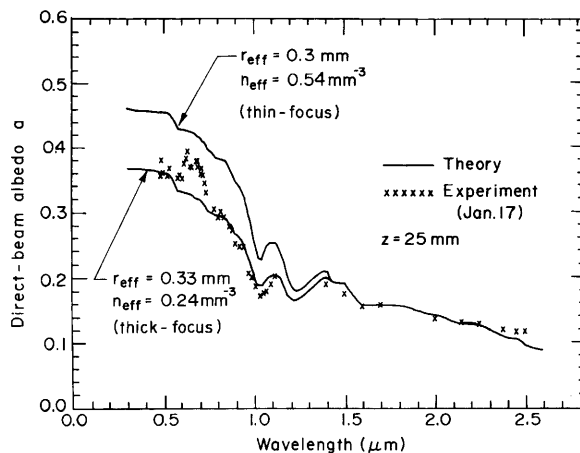


Fig. 16. Comparison of measured and calculated albedo of ice on Moses Lake, January 17, 1984, under clear sky. The two solid curves are computed using the two bubble size distributions plotted in Figure 15; they probably bracket the true size distribution. The solar zenith angle varied between 68° and 75° as the wavelength setting was changed during the experiment. The calculations at each wavelength assume a direct beam at the zenith angle which occurred during the measurement of that wavelength. The scatter at $\lambda < 0.7 \mu\text{m}$ is due to a failure of the wavelength determination system; reflected and incident measurements were not necessarily at the same wavelength.

calculations predict will be masked by the uncertainty in the bubble distribution. What is now needed are many measurements of bubble size distributions in natural ice, and a few experiments where both radiative properties and ice microstructure are measured.

Acknowledgments. We thank Thomas Grenfell for the use of his portable spectrophotometer, Warren Wiscombe for the use of his computer code for Mie-scattering, and both for helpful discussion. Craig Bohren critically reviewed the manuscript. Jack Kornfield at NSF encouraged us to undertake a study of lake ice because of its simplicity compared to sea ice. Some of the computations were done at the National Center for Atmospheric Research. The research was supported by NSF grants ATM-82-15337 and ATM-86-05134. The spectrophotometer is maintained with support from ONR contract N00014-84-C-0111.

REFERENCES

- Adams, W. P., Snow and ice on lakes, in *Handbook of Snow*, edited by D. M. Gray and D. H. Male, pp. 437-474, Pergamon, Elmsford, N. Y., 1981.
- Adams, W. P., and N. T. Roulet, Sampling of snow and ice on lakes, *Arctic*, 37, 270-275, 1984.
- Bari, S. A., and J. Hallett, Nucleation and growth of bubbles at an ice-water interface, *J. Glaciol.*, 13, 489-520, 1974.
- Bohren, C. F., Colors of snow, frozen waterfalls, and icebergs, *J. Opt. Soc. Am.*, 73, 1646-1652, 1983.
- Bohren, C. F., Multiple scattering of light and some of its observable consequences, *Am. J. Phys.*, 55, 524-533, 1987.
- Bohren, C. F., and D. P. Gilra, Extinction by a spherical particle in an absorbing medium, *J. Colloid Interface Sci.*, 72, 215-221, 1979.
- Bolsenga, S. J., Spectral reflectances of snow and fresh-water ice from 340 through 1100 nm, *J. Glaciol.*, 29, 296-305, 1983.
- Carte, A. E., Air bubbles in ice, *Proc. Phys. Soc.*, London, 77, 757-768, 1961.
- Chylek, P., Light scattering by small particles in an absorbing medium, *J. Opt. Soc. Am.*, 67, 561-563, 1977.
- Gavrilo, V. P., and B. Ya. Gaitskhoki, The statistics of air inclusions in ice, in *The Physics of Ice*, edited by V. V. Bogorodskii, pp. 125-128, translated from Russian by Israel Program for Scientific Translation, Jerusalem, 1970.
- Gow, A. J., and J. W. Govoni, Ice growth on Post Pond, 1973-1982, *USA CRREL Rep. 83-4*, 25 pp., Cold Reg. Res. and Eng. Lab., Hanover, N. H., 1983.
- Gow, A. J., and D. Langston, Growth history of lake ice in relation to its stratigraphic, crystalline and mechanical structure, *USA CRREL*

- Rep. 77-1, 24 pp., Cold Reg. Res. and Eng. Lab., Hanover, N. H., 1977.
- Grenfell, T. C., A visible and near-infrared scanning photometer for field measurements of spectral albedo and irradiance under polar conditions, *J. Glaciol.*, 27, 476-481, 1981.
- Grenfell, T. C., A theoretical model of the optical properties of sea ice in the visible and near infrared, *J. Geophys. Res.*, 88, 9723-9735, 1983.
- Grenfell, T. C., and G. A. Maykut, The optical properties of ice and snow in the Arctic basin, *J. Glaciol.*, 18, 445-463, 1977.
- Grenfell, T. C., and D. K. Perovich, Spectral albedos of sea ice and incident solar irradiance in the southern Beaufort Sea, *J. Geophys. Res.*, 89, 3573-3580, 1984.
- Hansen, J. E., and L. D. Travis, Light scattering in planetary atmospheres, *Space Sci. Rev.*, 16, 527-610, 1974.
- Houf, W. G., and F. P. Incropera, An assessment of techniques for predicting radiative transfer in aqueous media, *J. Quant. Spectrosc. Radiat. Transfer*, 23, 101-115, 1980.
- Irvine, W. M., Multiple scattering in planetary atmospheres, *Icarus*, 25, 175-204, 1975.
- Joseph, J. H., W. J. Wiscombe, and J. A. Weinman, The delta-Eddington approximation for radiative flux transfer, *J. Atmos. Sci.*, 33, 2452-2459, 1976.
- Knight, C. A., Slush on lakes, in *Structure and Dynamics of Partially Solidified Systems*, edited by D. E. Loper, pp. 455-465, Martinus Nijhoff, Dordrecht, The Netherlands, 1987.
- Marston, P. L., D. S. Langley, and D. L. Kingsbury, Light scattering by bubbles in liquids: Mie theory, physical-optics approximations, and experiments, *Appl. Sci. Res.*, 38, 373-383, 1982.
- Mullen, P. C., Spectral albedo of lake ice, M.S. thesis, 120 pp., Univ. of Wash., Seattle, 1984.
- Ragle, R. H., Formation of lake ice in a temperate climate, *USA CRREL Res. Rep. 107*, 24 pp., Cold Reg. Res. and Eng. Lab., Hanover, N. H., 1963.
- Saunderson, J. L., Calculation of the color of pigmented plastics, *J. Opt. Soc. Am.*, 32, 727-736, 1942.
- Swinzow, G. K., Ice cover of an arctic proglacial lake, *USA CRREL Res. Rep. 155*, 42 pp., Cold Reg. Res. and Eng. Lab., Hanover, N. H., 1966.
- Tanaka, M., and T. Nakajima, Effects of oceanic turbidity and index of refraction of hydrosols on the flux of solar radiation in the atmosphere-ocean system, *J. Quant. Spectrosc. Radiat. Transfer.*, 18, 93-111, 1977.
- van de Hulst, H. C., *Light Scattering by Small Particles*, 470 pp., John Wiley, New York, 1957.
- Walraven, R., Calculating the position of the sun, *Sol. Energy*, 20, 393-397, 1978.
- Warren, S. G., Optical constants of ice from the ultraviolet to the microwave, *Appl. Opt.*, 23, 1206-1225, 1984.
- Warren, S. G., and W. J. Wiscombe, A model for the spectral albedo of snow, II, Snow containing atmospheric aerosols, *J. Atmos. Sci.*, 37, 2734-2745, 1980.
- Wilkinson, B. J., An improved FORTRAN program for the rapid calculation of the solar position, *Sol. Energy*, 27, 67-68, 1981.
- Wilson, J. T., J. H. Zumberge, and E. W. Marshall, A Study of ice on an inland lake, *USA SIPRE Rep. 5*, 78 pp., Cold Reg. Res. and Eng. Lab., Hanover, N. H., 1954.
- Wiscombe, W. J., Mie scattering calculations: Advances in technique and fast, vector-speed computer modes, *Tech. Note, NCAR/TN-140 + STR* (NTIS PB 301388), Natl. Cent. for Atmos. Res., Boulder, Colo., 1979.
- Wiscombe, W. J., Improved Mie scattering algorithms, *Appl. Opt.*, 19, 1505-1509, 1980.
- Wiscombe, W. J., and S. G. Warren, A model for the spectral albedo of snow, I, Pure snow, *J. Atmos. Sci.*, 37, 2712-2733, 1980.

P. C. Mullen and S. G. Warren, Geophysics Program, AK-50, University of Washington, Seattle, WA 98195.

(Received August 27, 1987;
revised April 19, 1988;
accepted April 19, 1988.)